Journal of the Optical Society of Korea
Vol. 19, No. 3, June 2015, pp. 265-271

ISSN: 1226-4776(Print) / ISSN: 2093-6885(Online)
DOI: http://dx.doi.org/10.3807/JOSK.2015.19.3.265

Polarization-Dependent Microlens Array Using Reactive Mesogen Aligned by Top-Down Nanogrooves for Switchable Three-Dimensional Applications

Ki-Beom Son[1], Mugeon Kim[2], Min-Kyu Park[2], and Hak-Rin Kim[1,2]*

[1]*Department of Sensor and Display Engineering, Kyungpook National University, Daegu 702-701, Korea*
[2]*School of Electronics Engineering, Kyungpook National University, Daegu 702-701, Korea*

(Received April 20, 2015 : revised May 6, 2015 : accepted May 6, 2015)

We propose a reactive mesogen (RM) lens array to obtain good focusing behavior along with a short focal plane, where the focusing behavior is switchable according to the polarization state of incident light. Polarization-dependent focusing behavior is obtained using a planoconvex RM microlens array on a planoconcave isotropic lens template. Even though the sagitta of our RM lens is high, to obtain the short focal length, the RM layer can be aligned well by introducing a top-down alignment effect, using a nanogrooved template. The optical noise due to the moiré effect generated by the nanogrooves on the surface of the planoconvex RM layer can be removed simply by overcoating a thin RM layer, which is self-aligned by the geometric surface effect, without an additional alignment process. We demonstrate a hexagonal-packed RM lens array that has a very high fill factor and symmetric phase profile, for an ideal lens.

Keywords : Reactive mesogen, Switchable microlens, Switchable 3D applications, Overcoating process, Nanogrooves
OCIS codes : (160.3710) Liquid crystals; (230.3720) Liquid-crystal devices; (160.4760) Optical properties; (110.6880) Three-dimensional image acquisition; (330.1400) Vision - binocular and stereopsis

I. INTRODUCTION

Electrically switchable liquid crystal (LC) microlens arrays have been attracting much attention recently for a variety of three-dimensional (3D) applications, including 2D/3D switchable autostereoscopic 3D displays, integral photography, supermultiview 3D displays, and light-field cameras [1-5]. Most of these applications require an elemental lens with a short focal length, small pitch, high sagitta, and switchable nature [6-9]. In a light-field camera, for example, a photosensor array of fine pitch and a microlens array that is vanishingly small compared to the main lens are used to obtain images at various depths. To prevent image overlap and wasted pixels, the *f*-number of the main lens and microlens must be matched. Therefore, the focal length of the microlens should be less than several millimeters; in other words, the sagitta of the microlens array needs to be sufficiently large [10, 11].

Several types of LC lens have been introduced. One approach to fabricate a LC lens array is to make a gradient refractive index (GRIN) profile, in which the LC director is controlled by applying electric fields using patterned indium tin oxide (ITO) electrodes. In this case the focusing behavior deteriorates because the LC orientation is unstable in the center region between the electrodes, due to the reverse tilt distribution of the LC director. To utilize fringe-field distribution, the fill factor of the LC microlens array is also highly limited [12-14].

Another approach to a switchable lens is to use a planoconvex reactive mesogen (RM) lens array on a planoconcave isotropic lens template. The focusing behavior of the RM lens array can be switched by using the polarization state of an incident light, because an RM is an optically anisotropic material, like an LC. In this case the switching property between focused and defocused states can be obtained by using an additional polarization control layer. By separating polarization switching from polarization-dependent focusing, fast switching can be obtained with a low driving voltage.

*Corresponding author: rineey@ee.knu.ac.kr
Color versions of one or more of the figures in this paper are available online.

A polarization-dependent lens can also be made by aligning the LC instead of the RM; however, the LC layer needs two rigid substrates for stability, due to its inherent fluidity. An RM lens can be made on a single substrate, which enables the fabrication of an applicable thin-film optical element [15, 16].

Nevertheless, the use of an RM lens for some 3D applications is still limited, because these applications demand a short-focal-length microlens array with a small lens pitch. To obtain a short focal length with a small pitch, the sagitta and numerical aperture of the microlens must be increased, but when the thickness of the RM layer and the numerical aperture of the planoconcave lens template are increased, it is difficult to obtain a well-aligned thick RM layer with the planoconvex shape. This is because the alignment effect is reduced at the center and edge of the lens according to the increase in thickness, and the RM alignment is distorted by the highly curved planoconcave understructure.

In this paper we demonstrate a well-aligned polarization-dependent RM lens array by using top-down alignment due to nanogrooves for a geometric alignment effect [17, 18], along with conventional alignment methods such as a bottom-up LC alignment layer. In addition, we realize an RM lens that has a high fill factor because the edge region of the RM lens can be aligned well by top-down alignment. In this case, because of diffraction and moiré fringes caused by the remaining nanogroove structure on top of the RM layer, the imaging quality can be diminished [19, 20]. However, in our approach, by overcoating the same RM on the surface of the thick planoconvex RM layer, the polarization-dependent RM lens array can be planarized, providing an almost ideal lens profile.

II. FABRICATION OF THE RM LENS ARRAY

Figure 1 shows a schematic diagram of the proposed fabrication process for an RM lens array composed of three different layers: a planoconcave lens understructure made of UV-curable isotropic polymer, an LC alignment layer, and an RM layer. We used a hexagonal-packed spherical convex lens array template with a pitch of 250 μm and sagitta of 24 μm. First, the planoconcave lens was formed by nanoimprinting lithography using the UV-curable polymer NOA89 (n_p = 1.521, Norland Products Inc.), which is transparent in the visible region and optically isotropic; see Fig. 1(a). The template was treated by a UV-ozone process for 20 min, because the photocured polymer is hydrophobic. To form the alignment layer, a 2 wt% aqueous solution of polyvinyl alcohol (PVA) was coated after the UV-ozone process and thermally cured at 100°C for 20 min on the planoconcave lens template. The underlying polymer layer can be preserved well, because the annealing temperature of the PVA layer is low and the solvent is water, which is inert to the cross-linked NOA layer. To obtain bottom-up alignment, the PVA layer was bidirectionally rubbed to obtain a well-aligned RM layer and to avoid shading regions, especially in the spherical lens, as shown in Fig. 1(b). To make a polarization-dependent lens, we used an RM (RMM727, Δn = 0.192, Merck). The space between the bottom planoconcave lens template and the top polydimethylsiloxane (PDMS) mold, which had nanogrooves for geometric alignment, was filled with an RM layer by the one-drop filling process. Then UV light was irradiated for 90 s at 50 mW/cm^2 to cross-link the RM molecules, and the PDMS mold was peeled off after UV irradiation was complete, as shown in Fig. 1(c). After the PDMS mold was peeled off, the surface of the planoconvex RM layer was overcoated with a thin RM layer and UV cured, to prevent diffraction and moiré fringes due to the nanogrooves on top of the planoconvex RM layer.

RM molecules have an ordinary refractive index n_o and an extraordinary index n_e, like LC molecules. In our structure, when the polarization is parallel to the optical axis of the RM layer, the incident light is focused because n_e of the planoconvex RM layer is larger than the refractive index n_p of the optically isotropic planoconcave template, as shown in Fig. 2(a). On the other hand, when the polarization is orthogonal to the optical axis of the RM layer, the incident rays are not refracted, as shown in Fig. 2(b), because the ordinary refractive index of the RM and the index of the isotropic photocured polymer are the same ($n_o = n_p$).

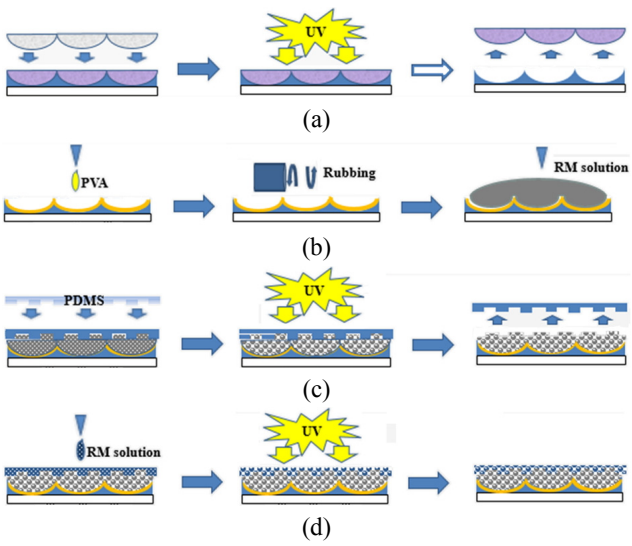

FIG. 1. Schematic diagram of the fabrication method for the RM lens: (a) nanoimprinting lithography to form the concave lens template made of UV-curable polymer; (b) one-drop filling process to form the RM layer after rubbing of the alignment layer for the bottom-up alignment condition; (c) top-down alignment by nanogrooves on the surface of the PDMS mold for the photopolymerizable convex RM layer, which is the polarization-dependent microlens array; and (d) overcoating process using RM solution, to prevent diffraction and moiré fringes due to nanogrooves on the surface of the planoconvex RM lens array after the PDMS mold is peeled off.

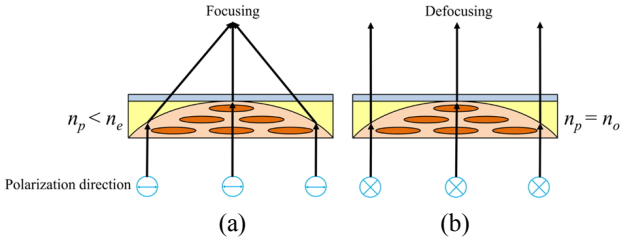

FIG. 2. Principle of (a) focusing and (b) defocusing of the proposed lens, depending on the incident polarization state using index mismatching ($n_e > n_p$), and index matching ($n_o = n_p$) conditions, respectively.

III. RESULTS AND DISCUSSION

Figure 3 shows polarizing-microscope images of the polarization-dependent RM lens array through crossed polarizers. The RM layer without top-down alignment is poorly aligned, because the anchoring energy of the bottom-up PVA layer alone is not sufficient to align all of the RM molecules, as shown in Fig. 3(a). In a conventional GRIN LC or RM lens, the molecular profile in the edge region is not well formed. Especially in our structure, the planoconcave undersubstrate has a high sagitta for the elemental lens array, which makes it very difficult to obtain a well-aligned RM layer. However, when the alignment of the RM layer is additionally supported by the top-down alignment effect, the RM layer is well aligned even in the sharp edge region, so the image is clearly dark when the polarizer and the direction of the RM molecules are set to be parallel, as shown in Fig. 3(b).

Figure 4 shows scanning electron microscope (SEM) images of the RM lens array. In our structure the UV-cured RM layer has nanogrooves on the surface after the peel-off process of the PDMS template, because the RM molecules were polymerized while preserving the conformal contact between the RM layer and PDMS nanogrooves to enhance the RM alignment, as shown in Fig. 4(b). The period of the nanogroove structure is 0.7 μm, and its width and height are 0.2 μm. The grooves could cause optical diffraction and moiré fringes, which diminished the imaging quality of the microlens. Figure 4(c) shows the SEM image after the nanogroove structure was overcoated with the same RM material to planarize the surface. The final structure has a very smooth surface, as shown in Fig. 4(a). The thickness of the overcoating layer was 1.3 μm, so the RM molecules were aligned well by the geometric alignment effect of the nanogroove structure, without any additional alignment method.

Figures 5(a) and 5(b) show the charge-coupled device (CCD) images focused on the surface of the RM lens array.

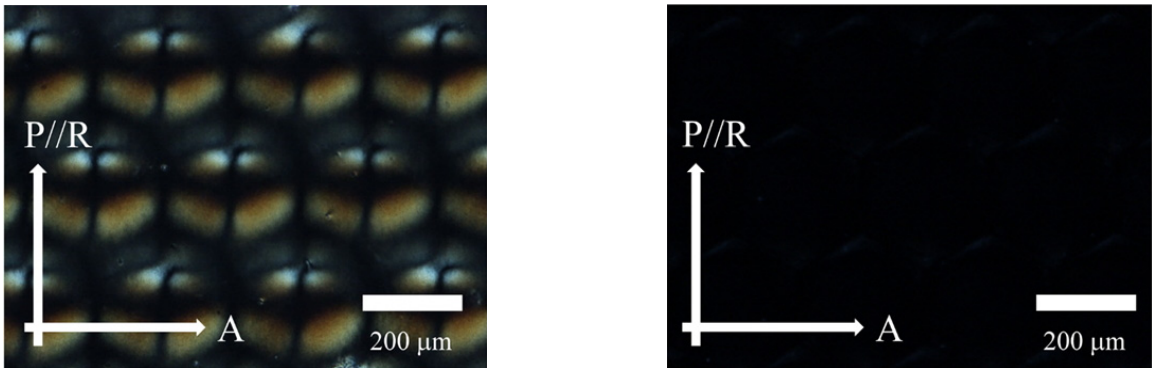

FIG. 3. Polarizing-microscope images showing the RM alignment texture when the rubbing direction of the PVA layer is parallel to the transmission axis of one of the polarizers: (a) RM layer aligned using only bottom-up alignment with the underlying rubbed PVA layer, and (b) RM layer aligned additionally by top-down geometric alignment effect using nanogrooves on the PDMS mold (P: bottom polarizer, R: optical axis of RM layer, A: top polarizer orthogonal to P).

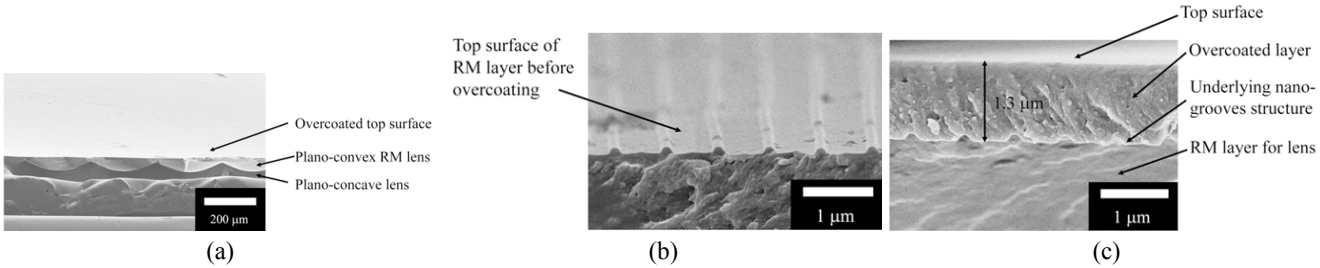

FIG. 4. Cross-sectional scanning electron microscopic images: (a) final structure of RM lens array with overcoated RM layer, (b) RM layer on the concave lens template before overcoating, and (c) enlarged image of (a) after overcoating with RM.

A fringe pattern caused by the moiré effect can be formed by superposition of periodic structures [19, 20]. In our case, because of the nanogroove structure the fringe pattern can be observed, as shown in Fig. 5(a). However, the fringe pattern disappeared after the overcoating process, as shown in Fig. 5(b). As mentioned previously, because of a fundamental problem, many LC lens designs have a low fill factor [9,11,13], but with our method we could obtain a microlens array with a high fill factor of more than 95%, as shown in Figs. 4(c) and 5(b).

A quantitative analysis of the imaging performance of the RM lens is needed to evaluate the effect of the moiré fringes. The modulation transfer function (MTF) is the most widely used scientific method for describing lens performance quantitatively [21]. The MTF is a measure of the transfer of modulation from the subject to the image. In other words, it measures how accurately the lens reproduces detail of the object in the image. To estimate the MTF of the polarization-dependent RM microlens array, we used the 1951 USAF resolution test chart. The MTF before overcoating was 0.172 and that after overcoating was 0.261 at 8.98 line pairs per millimeter, as shown in Fig. 6. In other words, the MTF was improved by 51.7% after the surface was planarized. Figures 5(c) and 5(d) show the images of the logo of our university after the RM lens array. The optical source was polarized parallel to the optical axis of the RM layer. The RM lens array before the overcoating process formed blurred images, as shown in Fig. 5(c), but

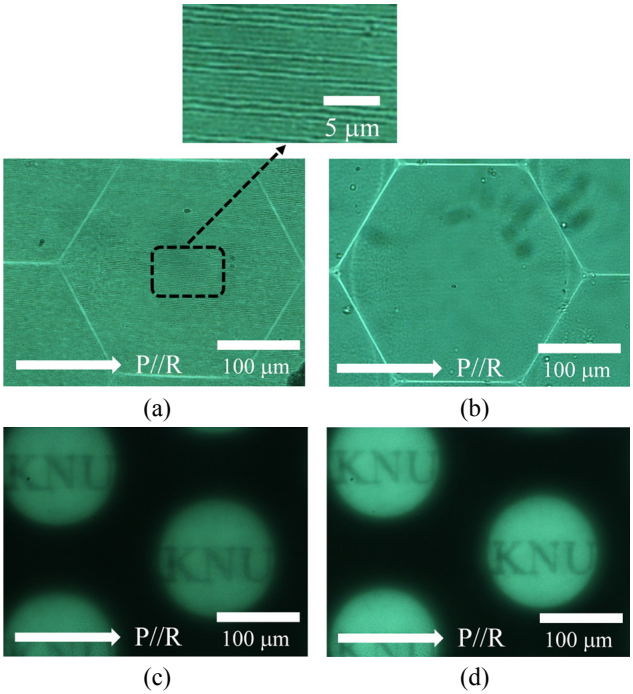

FIG. 5. CCD images focused on the hexagonal-packed RM lens array surface (a) before and (b) after overcoating. Images of the logo of our university ("KNU") observed at the image plane, with the RM lens array prepared (c) without and (d) with overcoating.

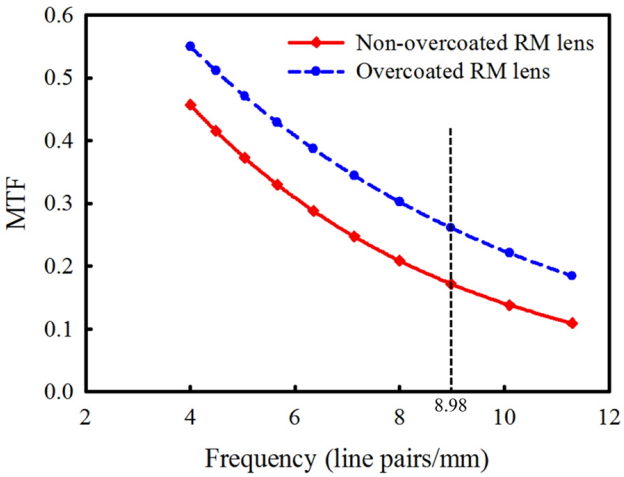

FIG. 6. MTF curves measured with the RM lens (red solid line with diamonds: non-overcoated RM lens, blue dashed line with circles: overcoated RM lens).

after the RM layer was overcoated with a thin RM layer, we could obtain clear images, as shown in Fig. 5(d).

Figure 7 shows the focusing and defocusing behavior of the polarization-dependent RM lens. When the polarization direction of the light and the rubbing direction of the alignment layer were parallel, the object image was clearly captured, as shown in Fig. 7(e), where the focal length of the RM lens array in Fig. 7(a) was 2 mm. Assuming that the optical axis of the RM layer is along the x-axis, the x-component of the polarized light is focused, and the y-component is defocused. Therefore, when the polarization direction deviates from the alignment direction of the RM layer, the focused beam intensity is reduced, as shown in Figs. 7(a)-(d). These result in more blurry object images, as shown in Figs. 7(e)-(h). When the polarization directions of the incident beam and optical axis of the RM layer were orthogonal, the RM lens was completely defocused, without generating any object image, as shown in Figs. 7(d) and 7(h).

We measured the intensity profile at the focal plane, for quantitative analysis in addition to the qualitative analysis of the RM lens performance. Figure 8 shows the relative intensity profile of the light focused by the RM lens. Because of diffraction and scattering by the nanogrooves on the uncoated RM lens, the peak intensity was lower than that of the overcoated RM lens. This graph shows that the nanogrooves can adversely affect the focusing efficiency, even though the RM alignment itself can be further improved by the additional top-down alignment effect.

Figure 9(a) shows a polarizing-microscope image of the polarization-dependent RM lens array placed between two crossed polarizers. The optical axis of the RM molecules was oriented at 45° with respect to the bottom polarizer. Because of the birefringence of the RM layer, the dark

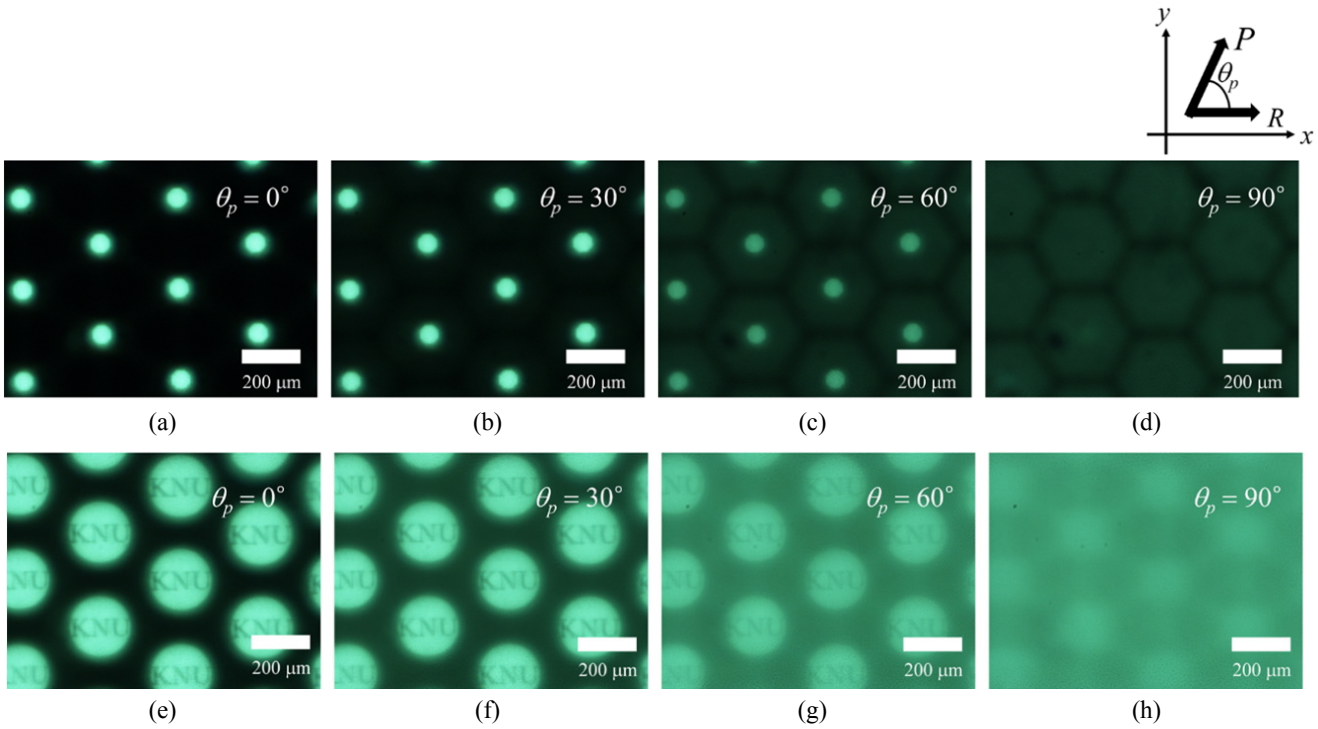

FIG. 7. (a), (b), (c), and (d): CCD images at the focal plane, showing the focusing behavior of the polarization-dependent RM lens array according to the polarization condition; (e), (f), (g), and (h): CCD images at the image plane showing the imaging behavior of the polarization-dependent RM lens array according to the polarization condition.

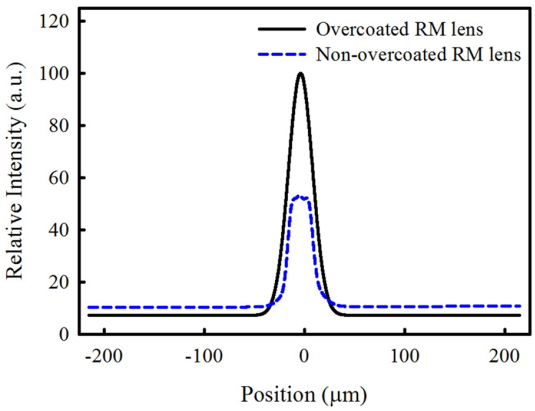

FIG. 8. Focused beam intensity profiles of the overcoated RM lens (black solid line) and the non-overcoated RM lens (blue dashed line).

concentric-circle pattern can be observed at the positions where the degree of phase retardation is equal to integer multiples of 2π. Unlike that of a conventional LC or RM lens, the phase profile of our lens was very circularly symmetric, even at the sharp lens edges, as shown in Fig. 9(a). We calculated the relative phase retardation profile ($\Delta\Gamma$) of the RM layer from the dark concentric rings, as shown in Fig. 9(b), where the scaled parameter α is defined as $\alpha = \Delta\Gamma 2/\pi$. In Fig. 9(b), the ideal phase profile, which is obtained assuming that the RM molecules are perfectly aligned

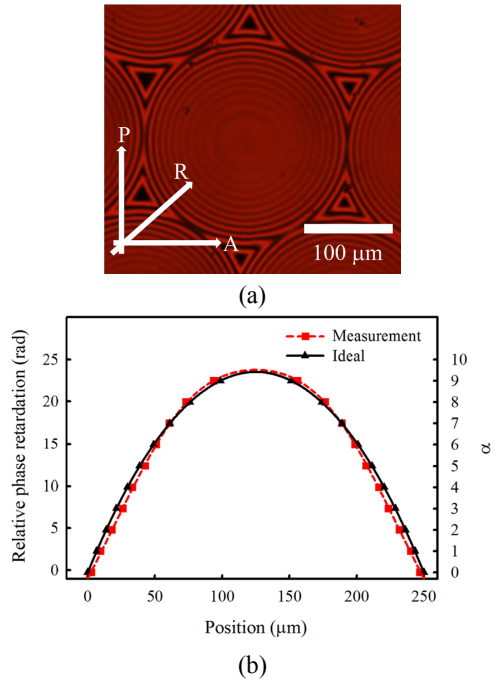

FIG 9. (a) Polarizing-microscope image of the overcoated RM lens array, and (b) relative phase retardation profile across the overcoated RM lens aperture, which is obtained from the black concentric ring patterns in (a) (red dashed line with squares), and the result calculated assuming that the RM molecules are unidirectionally aligned without orientational distortion (black solid line with triangles).

without any distortion, is also plotted. From the two phase profiles, the error function for quantitative analysis can be defined as follows [22, 23]:

$$EF = \sqrt{\frac{\sum_{j}^{n}\left(\Gamma_j^m - \Gamma_j^i\right)^2}{n}} \times 100\% \quad (1)$$

where n is the number of black concentric circles, and Γ_j^m and Γ_j^i are the measured phase retardation of the RM lens and the ideal phase retardation. The error from Equation (1) was sufficiently small, 14.29%, for our structure. However, even with our top-down alignment effect, the effective extraordinary refractive index of the RM layer became slightly smaller than the original refractive index in the edge region of the concave template, as shown in Fig. 9(b).

IV. CONCLUSION

We demonstrated a polarization-dependent microlens array where the alignment property of the planoconvex RM layer was much improved by an additional top-down alignment effect with a nanogroove pattern. The optical noise from the nanogroove on the planoconvex RM lens surface could be easily removed by additional overcoating with a thin RM layer, utilizing the geometrical alignment effect once again. Our fabrication method showed that the phase profile of the RM lens became almost the same with an ideal phase profile at the microlens array conditions of 250 μm in lens pitch, 2 mm in focal length, and over 95% fill factor. With the improved RM alignment property of our approach, a planar-concave template with a higher curvature can be used as the underlying substrate for a polarization-dependent RM lens array with a lower *f*-number. Currently, a switchable RM lens array with a shorter focal length (< *f*/4) is under design and fabrication, even after considering the effect of the spherical aberration for a more accurate imaging property, which will be presented in a later report. Such a microlens array using RM has potential applications in 2D/3D switchable autostereoscopic 3D displays, integral photography, super multiview 3D displays, and light-field cameras.

ACKNOWLEDGMENT

This research was financially supported by the "Over regional linked 3D convergence industry promotion program" through the Ministry of Trade, Industry&Energy(MOTIE) and Korea Institute for Advancement of Technology(KIAT) (No.R0001519).

REFERENCES

1. S. Sato, "Liquid-crystal lens-cells with variable focal length," Jpn. J. Appl. Phys. **18**, 1679-1684 (1979).
2. H.-K. Hong, S.-M. Jung, B.-J. Lee, H.-J. Im, and H.-H. Shin, "25.3: Autostereoscopic 2D/3D switching display using Electric-Field-Driven LC Lens (ELC Lens)," in *Proc. SID Symp. Tech. Dig.* (Los Angeles Convention Center, Los Angeles, California, USA, May 2008), vol. 39, pp. 348-351.
3. Y.-P. Huang, C.-W. Chen, and Y.-C. Huang, "Superzone Fresnel liquid crystal lens for temporal scanning auto-stereoscopic display," J. Disp. Tech. **8**, 650-655 (2012).
4. J. Kim, S.-U. Kim, B.-Y. Lee, J.-H. Suh, and S.-D. Lee, "Lenticular lens array based on liquid crystal with a polarization-dependent focusing effect for 2D-3D image applications," J. Inf. Disp. **16**, 11-15 (2015).
5. B. Song and S. W. Min, "2D/3D convertible integral imaging display using point light source array instrumented by polarization selective scattering film," J. Opt. Soc. Korea **17**, 162-167 (2013).
6. J.-Y. Son, V. V. Saveljev, Y.-J. Choi, J.-E. Bahn, S.-K. Kim, and H. Choi, "Parameters for designing autostereoscopic imaging systems based on lenticular, parallax barrier, and integral photography plates," Opt. Eng. **42**, 3326-3333 (2003).
7. M. Hain, R. Glöckner, S. Bhattacharya, D. Dias, S. Stankovic, and T. Tschudi, "Fast switching liquid crystal lenses for a dual focus digital versatile disc pickup," Opt. Commun. **188**, 291-299 (2001).
8. C.-W. Chiu, Y.-C. Lin, P. C.-P. Chao, and A. Y.-G. Fuh, "Achieving high focusing power for a large aperture liquid crystal lens with novel hole-and-ring electrodes," Opt. Express **16**, 19277 (2008).
9. D.-Y. Yoon, T.-W. Kim, M. Kim, and H.-J. Pahk, "Unambiguous 3D surface measurement method for a micro-Fresnel lens-shaped lenticular lens based on a transmissive interferometer," J. Opt. Soc. Korea **18**, 37-44 (2014).
10. J. Arai, H. Kawai, and F. Okano, "Microlens arrays for integral imaging system," Appl. Opt. **45**, 9066-9078 (2006).
11. R. Ng, M. Levoy, M. Brédif, G. Duval, M. Horowitz, and P. Hanrahan, "Light field photography with a hand-held plenoptic camera," Stanford Technical Report CTSR 2005-02 (2005).
12. C.-W. Chen, Y.-P. Huang, and P.-C. Chen, "Dual direction overdriving method for accelerating 2D/3D switching time of liquid crystal lens on auto-stereoscopic display," J. Disp. Tech. **8**, 559-561 (2012).
13. H. Ren, D. W. Fox, B. Wu, and S.-T. Wu, "Liquid crystal lens with large focal length tunability and low operating voltage," Opt. Express **15**, 11328-11335 (2007).
14. Y.-H. Fan, H. Ren, and S.-T. Wu, "Switchable Fresnel lens using polymer-stabilized liquid crystals," Opt. Express **11**, 3080-3086 (2003).
15. H.-C. Lin and Y.-H. Lin, "An electrically tunable-focusing liquid crystal lens with a low voltage and simple electrodes," Opt. Express **20**, 2045-2052 (2012).
16. Y.-H. Lin, M.-S. Chen, and H.-C. Lin, "An electrically tunable optical zoom system using two composite liquid crystal lenses with a large zoom ratio," Opt. Express **19**, 4714-4721 (2011).
17. D. Berreman, "Solid surface shape and the alignment of an adjacent nematic liquid crystal," Phys. Rev. Lett. **28**, 1683-1686 (1972).
18. Y. Choi, H. Yokoyama, and J. S. Gwag, "Determination of

surface nematic liquid crystal anchoring strength using nano-scale surface grooves," Opt. Express **21**, 12135-12144 (2013).
19. Y. Kim, G. Park, J.-H. Jung, J. Kim, and B. Lee, "Color moiré pattern simulation and analysis in three-dimensional integral imaging for finding the moiré-reduced tilted angle of a lens array," Appl. Opt. **48**, 2178-2187 (2009).
20. R.-S. Chang, J.-Y. Sheu, C.-H. Lin, and H.-C. Liu, "Analysis of CCD Moiré pattern for micro-range measurements using the wavelet transform," Opt. Laser Tech. **35**, 43-47 (2003).
21. L. Li, D. Bryant, T. V. Heugten, and P. J. Bos, "Near-diffraction-limited and low-haze electrooptical tunable liquid crystal lens with floating electrodes," Opt. Express **21**, 8371-8381 (2013).
22. Y.-P. Huang, C.-W. Chen, and T.-C. Shen, "High resolution autostereoscopic 3D display with scanning Multi-Electrode Driving Liquid Crystal (MeD-LC) lens," in *Proc. SID Symp. Tech. Dig.* (Henry B. Gonzalez Convention Center, San Antonio, Texas, USA, June 2009), vol. 40, pp. 336-339.
23. C.-W. Chen, Y.-C. Huang, Y.-P. Huang, and J.-F. Huang, "Fast switching Fresnel liquid crystal lens for autostereoscopic 2D/3D display," in *Proc. SID Symp. Tech. Dig.* (Washington State Convention Center, Seattle, Washington, USA, May 2010), vol. 41, pp. 428-431.